Journal of Advanced Ceramics
2013, 2(3): 266–273
DOI: 10.1007/s40145-013-0070-0

ISSN 2226-4108
CN 10-1154/TQ

Research Article

Hydrothermal synthesis and characterization of $MnCo_2O_4$ in the low-temperature hydrothermal process: Their magnetism and electrochemical properties

Lianfeng DUAN[a,b,*], Fenghui GAO[a], Limin WANG[b], Songzhe JIN[a], Hua WU[a]

[a]*Key Laboratory of Advanced Structural Materials*, *Ministry of Education*, *and Department of Materials Science and Engineering*, *Changchun University of Technology*, *Changchun 130012*, *China*
[b]*State Key Laboratory of Rare Earth Resource Utilization*, *Changchun Institute of Applied Chemistry*, *Chinese Academy of Sciences*, *Changchun 130022*, *China*

Received: April 18, 2013; Revised: May 14, 2013; Accepted: May 15, 2013

Abstract: $MnCo_2O_4$ octahedral structure with edge length about 500 nm was successfully synthesized by a simple hydrothermal route. With the use of NaOH, the chemical potential and the rate of ionic motion in the precursor solution were controlled, and the particle size was limited. The magnetization measurements revealed that the products exhibited ferrimagnetic characteristics with different saturation magnetization and coercivity at different measuring temperatures. In addition, the as-prepared $MnCo_2O_4$ as anodes for lithium-ion batteries (LIBs) exhibited a reversible capacity of 1180 mA·h/g and 1090 mA·h/g at current density of 0.1 C and 1 C, respectively. The excellent cyclic performance was confirmed because the value of reversible capacity for $MnCo_2O_4$ was 618 mA·h/g after 50 cycles at 0.1 C. Owing to the good rate performance, $MnCo_2O_4$ octahedral products were suggested to have a promising application as anode material for LIBs.

Keywords: $MnCo_2O_4$; hydrothermal synthesis; lithium-ion batteries (LIBs); anode

1 Introduction

Complex oxides (containing two or more types of cations) with spinel structure under controlled size and shape are of intense interests for both fundamental science and technological applications because of their chemical and physical properties [1–3]. Among these, transition-metal cobaltites having a spinel structure MCo_2O_4 (M = Mn, Ni, Zn) with unusual physicochemical properties are widely used in many areas such as colossal magnetoresistance (CMR), sensors, fuel cell electrodes, electrical catalysts, microwave adsorption, etc. [4–7]. In particular, lithium-ion batteries (LIBs) have become the main power source for today's portable electronics and are being actively pursued for propelling electric vehicles in the near future. However, to match the growing demand for LIBs, higher discharge capacity is needed. Meanwhile, renewed interest in transition-metal oxides as potential anode materials for use in LIBs starts to grow [8,9]. Compared with graphite (372 mA·h/g), transition-metal cobaltites can deliver a high specific capacity. It has been reported that the mixed transition-metal oxides including $NiCo_2O_4$ [10], $ZnCo_2O_4$ [11] and $MnCo_2O_4$ [12] have been applied as anode materials for LIBs. Among these

* Corresponding author.
E-mail: duanlf@mail.ccut.edu.cn

transition-metal oxides, spinel $MnCo_2O_4$ has been studied widely due to it promising applications as a magnetic material. However, as an anode material for LIBs, $MnCo_2O_4$ has received little attention. $MnCo_2O_4$ particles have been prepared by various approaches such as Pechini method, sol–gel techniques, coprecipitation, microwave plasma synthesis, milling the oxide powders ($MnCO_3$ and Co_3O_4), spray pyrolysis of the metal nitrate aqueous solutions, heat mixture of $MnCO_3$ and CoC_2O_4, and so on [13–16]. However, the research on $MnCo_2O_4$ particles into different architectures and their structural development are comparatively limited, because the size, morphology, composition, dispersion, and surface features of the particles cannot meet the needs of further practical applications.

Up to now, reports on the morphology-controlled synthesis of $MnCo_2O_4$ through an aqueous reduction strategy under mild conditions is still lacked. The hydrothermal method demonstrates its superiority in controlling the shape of crystals [17]. In this paper, we present the synthesis of octahedral $MnCo_2O_4$ via a facile hydrothermal process. The influences of reaction time, dosage of sodium hydroxide on the morphology of the products have been investigated. To compare these results with that of a low ferrimagnetic oxide system, we have examined the magnetic behavior of $MnCo_2O_4$. The electrochemical performance of the as-prepared powders was also evaluated. By the studying of the charge–discharge properties of the submicrocrystals with octahedral structure, it can be expected that $MnCo_2O_4$ could be used as anode material for LIBs in future applications.

2 Experimental section

All chemicals of analytical grade were used without further purification. In the first step, 0.2745 g $Co(NO_3)_2$ was dissolved in 20 ml EG (ethylene glycol) under magnetic stirring at room temperature. Then 0.0527 g $KMnO_4$ and different dosages of NaOH were also added sequentially with constant magnetic stirring. The mixture was transferred into a 30 ml stainless steel autoclave, sealed, and maintained at 200 ℃ for 24 h. After completion of the reaction, the products were collected by centrifuge separation, washed several times with water and absolute ethanol, and finally dried in a vacuum oven at 40 ℃ for 6 h.

The phases were identified by means of X-ray diffraction (XRD) using a Rigaku D/max 2500pc X-ray diffractometer with Cu Kα radiation ($\lambda = 1.54156$ Å) at a scan rate of 0.04 (°)/s. The morphologies were characterized by a JEOL JSM-6700F field-emission scanning electron microscope (FESEM) operated at an acceleration voltage of 8.0 kV. Transmission electron microscopy (TEM), high-resolution TEM (HRTEM) observations, and selected-area electron diffraction (SAED) patterns were obtained by using a JEOL 2100F instrument with an emission voltage of 200 kV. Magnetic measurements were carried out using a Quantum Design superconducting quantum interference device (SQUID) magnetometer (LakeShore 7307).

The electrochemical experiments were performed via CR2025 coin-type test cells assembled in a dry argon-filled glove box with both moisture and oxygen contents below 1 ppm. The test cell consisted of a working electrode and lithium foil which were separated by a Celgard 2400 membrane. The electrolyte solution was prepared by dissolving 1 M $LiPF_6$ in EC-DMC (ethylene carbonate dimethyl carbonate) (weight-to-weight ratio = 1:1). The working electrodes were prepared by casting slurry containing 80% active material, 10% acetylene black and 10% polyvinylidene fluoride (PVDF) onto a copper foil. After vacuum drying at 80 ℃ for about 12 h, the electrode disks ($d = 12$ mm) were punched and weighed. Each electrode has approximately 1–3 mg active material. Galvanostatic charge–discharge cycling tests were performed using an LAND CT2001A multi-channel battery testing system in the voltage range between 0.5 V and 3 V at room temperature.

3 Results and discussion

The XRD pattern of the as-obtained $MnCo_2O_4$ crystals is shown in Fig. 1. All the diffraction peaks in the XRD pattern of the products can be indexed to the face-centered cubic structure of $MnCo_2O_4$ (JCPDS 23-1237). The sharpness of the XRD peaks confirms that the material should be highly crystallized $MnCo_2O_4$ without any other impurities. Further insight into the morphology and microstructure of the $MnCo_2O_4$ octahedra was gained by using FESEM and TEM. Figure 2 shows the typical FESEM and TEM images of $MnCo_2O_4$ ferrite crystals, from which we can conclude that octahedral structures are the

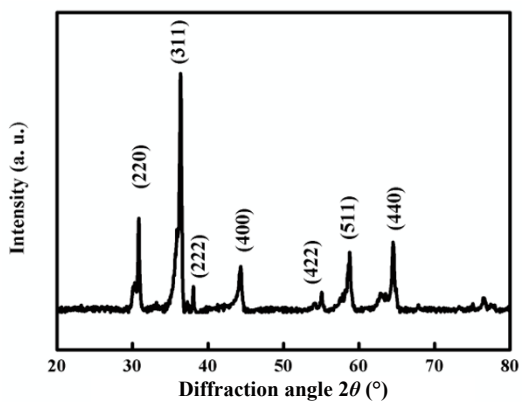

Fig. 1 XRD pattern of the as-obtained products.

exclusive products, which means that the $MnCo_2O_4$ octahedra can be prepared on a large scale. From the high-magnification FESEM and TEM images of the products (Figs. 2(b) and 2(c)), the edge length of octahedral $MnCo_2O_4$ crystals is about 500 nm. HRTEM was performed on an individual $MnCo_2O_4$ particle, as shown in Fig. 2(d). The clear and alignment of lattice fringes demonstrate that the octahedron is essentially single crystalline with no crystal defects. The lattice spacing between two adjacent fringes that can be observed corresponds to the set of $(1\bar{1}1)$ planes with a lattice spacing of 0.238 nm and the set of (220) planes with a lattice spacing of 0.293 nm, respectively. In principle, a crystal growth process consists of nucleation and growth, which are affected by the intrinsic crystal structure and external conditions. It is well known that spinel $MnCo_2O_4$ is cubic in structure, and the well defined octahedral morphology is characteristic of cubic structured crystals bound by eight (111) planes. Because of the slow reaction rate under the present hydrothermal synthesis conditions and the absence of other structure-modifying ions, octahedra with entirely {111} faces are considered to be the thermodynamically favorable product structures [18].

The corresponding inverse fast-Fourier-transform (FFT) pattern and the filtered FFT of a selected area of the image are shown in the insets of Fig. 2(d). It represents a pattern of diffraction spots with hexagonal

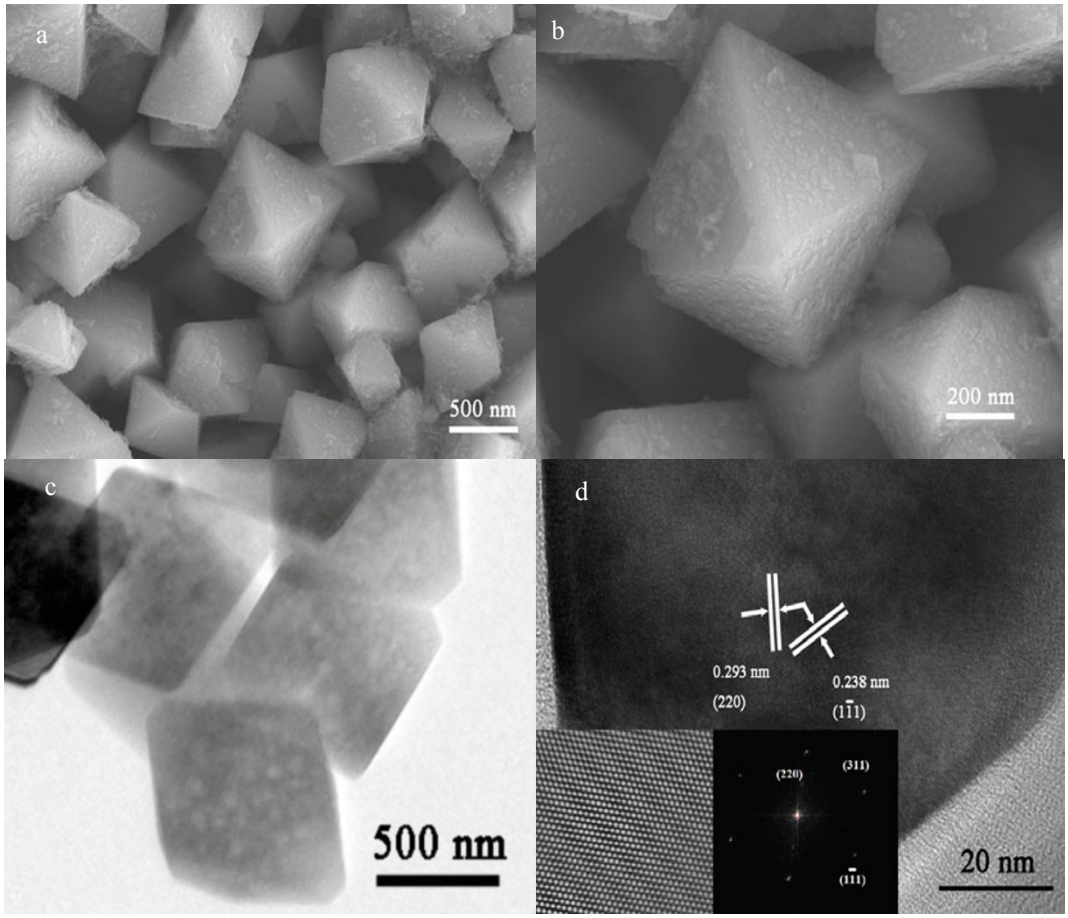

Fig. 2 FESEM image of the as-prepared products: (a) low magnification and (b) high magnification; (c) TEM and (d) HRTEM. The insets are filtered FFT (left) and inverse FFT (right) of the HRTEM image.

symmetry. The FFT pattern illustrates a perfect single crystal nature of the $MnCo_2O_4$, where the spots can be steadily indexed to (220), (311), $(1\bar{1}1)$ facets. And from the filtered FFT image which is just several atom distance wide, the atoms are aligned which means there is not any dislocation. It is further confirmed that the $MnCo_2O_4$ submicrocrystals are single crystalline.

To understand the formation mechanism of the octahedral $MnCo_2O_4$ particles, alkalinity-dependent experiments were carried out. Herein, Fig. 3 shows the SEM images of the samples obtained at various dosages of NaOH at 200 ℃ for 24 h. In fact, irregular particles are obtained when the dosage of NaOH is 0.4 g. With the increase in NaOH concentration, the morphology of the products evolves into a perfect octahedral structure with few irregular particles. When the amount of NaOH is increased to 1 g, it is interesting to note that the morphology of particles presents an octahedral shape (Fig. 2). The higher chemical potential is mainly determined by the concentration of NaOH. The pH value is supposed to exert an impact on both the rates of crystal nucleation and crystal growth [19]. Peng and Peng [20,21] have elucidated the influence of chemical potential on the shape evolution. The hydroxide with high concentrations is easily adsorbed onto (111) facets, which are then stabilized and grow slowly; hence, the growth of other facets will gradually diminish [22]. The alkalinity affects the balance between the chemical potential and the rate of ionic motion in the precursor solution, and a high concentration of NaOH accelerates the nucleation [23]. Especially, nucleation and aggregation growth in the EG solution are kinetically slower than those in the aqueous solution due to fewer surface hydroxyls and greater viscosity, thus allowing the particles to rotate adequately to find the low-energy configuration interface and form assemblies [24]. With the low concentration of hydroxide, $MnCo_2O_4$ can no longer be formed. In this case, $Co(OH)_3$ and $Mn(OH)_2$ deposit first, then complex compounds with Co^{3+} and Mn^{2+} are formed. So, with the increase of hydroxide we speculate that the redox reaction between MnO_4^-

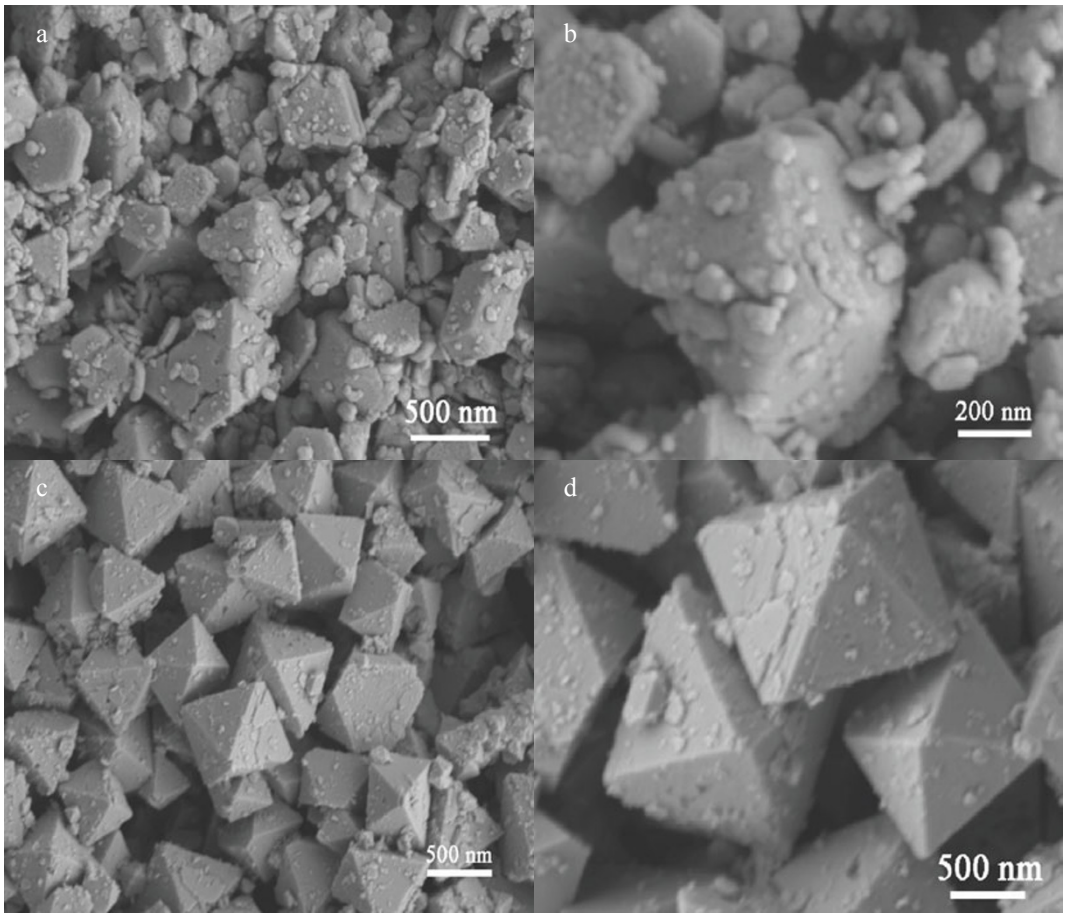

Fig. 3 FESEM images of the samples prepared with different dosages of NaOH: (a) low magnification and (b) high magnification of 0.4 g; (c) low magnification and (d) high magnification of 0.8 g.

and Co^{2+} in alkaline solution is very important. The chemical reaction in the hydrothermal process can be written as follows:

$$4MnO_4^- + 8Co^{2+} + 12OH^- \rightarrow 4MnCo_2O_4 + 3O_2 \uparrow + 6H_2O$$

From the formula, the final product is strongly dependent on the mole ratio of MnO_4^- and Co^{2+}, which should be 1:2 for the formation of $MnCo_2O_4$. From the above experimental results, the hole is formed, where the gases produced in reaction solution with the dosage of 1 g NaOH destroy the interior of loose aggregates from the chemical formula. It is further verified for the rough surface of particles. With increasing in the reaction time, Ostwald ripening process should gradually replace the aggregation-based crystal growth due to the increasing size difference between the center and outer parts of aggregates, which could recover the hole under the crystal growth (Fig. 4). And it seems that the concentration of NaOH plays a key role in the microstructures of the final products. Both high concentration of OH^- ions and high chemical potential in solution favor the growth of octahedral structures over other possible crystal forms.

In order to further understand the growth evolution of the $MnCo_2O_4$ microcrystals, the effect of the reaction time (3 h, 6 h, 12 h and 18 h) was systematically investigated. The FESEM images of the samples are shown in Fig. 4 as a function of reaction time. At the initial step of the reaction (Fig. 4(a)), a few small $MnCo_2O_4$ nucleuses are formed due to redox reaction between MnO_4^-, Co^{2+} and OH^-. As thermodynamic growth occurs, there is physical adsorption of the diffusing nanoparticles once they are in contact with one another. When the reaction time is increased to 6 h, the aggregated particles with irregular shape are formed, as shown in Fig. 4(b). When it is extended to 12 h, the embryo octahedra already generate, because Ostwald ripening process would gradually replace the aggregation-based crystal growth in order for the increasing size. If the hydroxy groups are adsorbed on some areas of its surface, the growth rate of crystal in certain directions will be confined. Due to the gases produced, the hole is formed at the particle surface from Fig. 4(c). After 18 h, the relatively octahedral microcrystal is synthesized, and

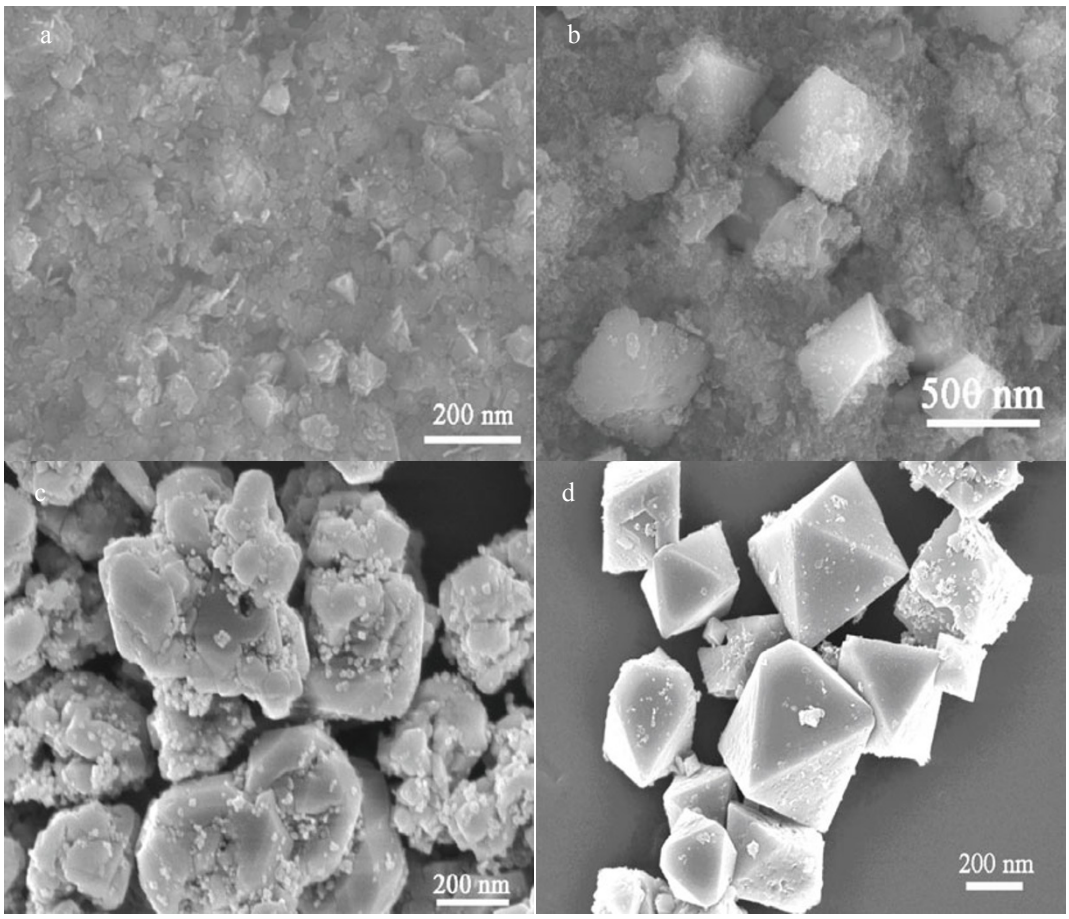

Fig. 4 FESEM images of the samples prepared under different reaction time: (a) 2 h; (b) 6 h; (c) 12 h; (d) 18 h.

the edge length of $MnCo_2O_4$ octahedra is 300 nm. At last, the typical octahedral morphology character of the $MnCo_2O_4$ is observed at 24 h.

The magnetic properties of $MnCo_2O_4$ microcrystals, which were tested at 300 K and 2 K by SQUID are shown in Fig. 5. The saturation magnetization (M_s) and coercivity (H_c) values of $MnCo_2O_4$ nanooctahedra are 0.649 emu/g and 0.657 emu/g, 64.68 Oe and 168.56 Oe at 300 K and 2 K, respectively. In addition, the H_c of the samples at 2 K are larger than those at 300 K due to the reduced influence of thermal fluctuation on the rotation of magnetic dipoles. Such a rearrangement would give rise to a small distortion of the structure and affect the local ordering of the ions in the octahedral sites. Further detailed investigation is required to understand the unusual magnetic hysteresis behavior of $MnCo_2O_4$.

The as-prepared $MnCo_2O_4$ particles are then tested as anodes for LIBs. The typical first charge–discharge profiles of anode material of $MnCo_2O_4$ particles at a current density of 0.1 C are shown in Fig. 6(a). The initial discharge is 1180 mA·h/g, which is almost four times higher than that of the common carbonaceous materials. The discharge voltage plateau at about 0.7 V is quite stable. The electrochemical mechanism of the $MnCo_2O_4$ electrode obeys to the displacive redox mechanism confirmed by many researchers [25–27].

$$MnCo_2O_4 + 8Li^+ + 8e^- \rightarrow 2CoO + MnO_2 + 8Li$$

$$2CoO + MnO_2 + 8Li \rightarrow MnCo_2O_4 + 8Li^+ + 8e^-$$

Figure 6(b) shows the charge–discharge capacities versus cycle number and efficiency for the $MnCo_2O_4$ at current densities of 0.1 C and 1 C between 0.50 V and 3.00 V (vs. Li/Li^+) at room temperature. Discharge capacities obtained for the second cycle at 0.1 C is 1060 mA·h/g. After 50 cycles, polyhedron structure remains about 618 mA·h/g, which is much larger than the other structure particles. Even at a high current density of 1.0 C, a discharge capacity of 380 mA·h/g is retained after 50 cycles. Although this value is much lower than those of the earlier cycles, it is still higher than the other transition-metal oxides, such as Co_3O_4, $CoFe_2O_4$ and $MnFe_2O_4$ [28]. The improved electrochemical performance makes such $MnCo_2O_4$ different structure promising as anode material for next-generation LIBs.

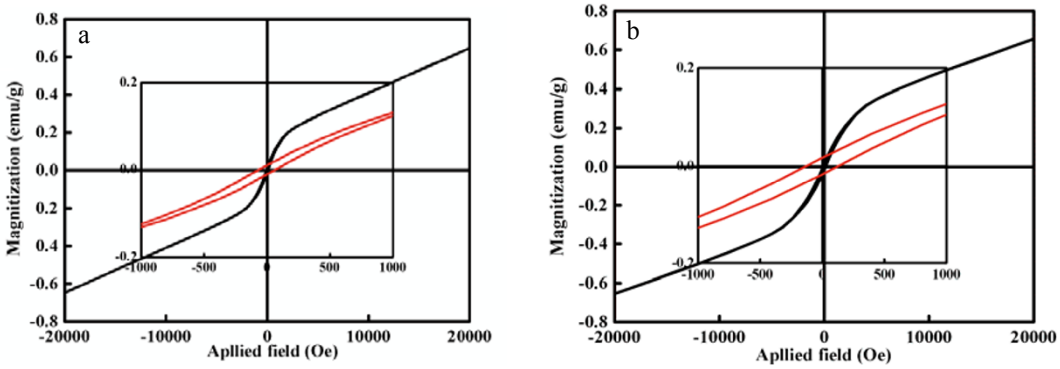

Fig. 5 Magnetization curves measured at different temperatures: (a) 300 K; (b) 2 K.

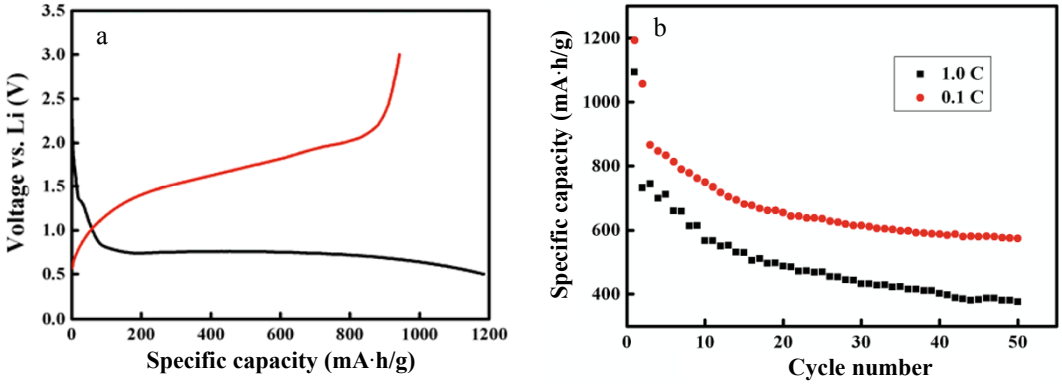

Fig. 6 (a) Charge–discharge plots and (b) cyclic performance of the $MnCo_2O_4$ electrode at a current density of 0.1 C and 1.0 C between 0.50 V and 3.00 V (vs. Li/Li^+) at room temperature.

4 Conclusions

In summary, $MnCo_2O_4$ octahedra have been successfully prepared via a facile hydrothermal synthetic approach. It has been found that the concentration of hydroxide ions plays a key role in control of size, morphology and structure of the products, which affect the balance between the chemical potential and the rate of ionic motion in the precursor solution, and the hydroxide with high concentration could be adsorbed onto (111) facets easily. It has been observed that the H_c of the samples at 2 K are much larger than that at room temperature by magnetization curve. In addition, the as-prepared $MnCo_2O_4$ as anodes for LIBs exhibits a reversible capacity of 1180 mA·h/g at a current density of 0.1 C, retaining 618 mA·h/g after 50 cycles. The results show that the as-prepared $MnCo_2O_4$ octahedral microcrystal is a kind of promising anode material for LIBs.

Acknowledgements

This work was supported by the Natural Science Foundation of Jilin Province (201215118) and the Special Funds of Changchun University of Technology.

References

[1] Hinklin TR, Azurdia J, Kim M, *et al*. Finding spinel in all the wrong places. *Adv Mater* 2008, **20**: 1373–1375.

[2] Yoon TJ, Kim JS, Kim BG, *et al*. Multifunctional nanoparticles possessing a “magnetic motor effect” for drug or gene delivery. *Angew Chem Int Edit* 2005, **44**: 1068–1071.

[3] Marco JF, Gancedo JR, Gracia M, *et al*. Cation distribution and magnetic structure of the ferrimagnetic spinel $NiCo_2O_4$. *J Mater Chem* 2001, **11**: 3087–3093.

[4] Rios E, Gautier J-L, Poillerat G, *et al*. Mixed valency spinel oxides of transition metals and electrocatalysis: Case of the $Mn_xCo_{3-x}O_4$ system. *Electrochim Acta* 1998, **44**: 1491–1497.

[5] Nissinen T, Kiros Y, Gasik M, *et al*. Comparison of preparation routes of spinel catalyst for alkaline fuel cells. *Mater Res Bull* 2004, **39**: 1195–1208.

[6] Zhu J, Gao Q. Mesoporous MCo_2O_4 (M = Cu, Mn and Ni) spinels: Structural replication, characterization and catalytic application in CO oxidation. *Microporous Mesoporous Mater* 2009, **124**: 144–152.

[7] Zhao D-L, Lv Q, Shen Z-M. Fabrication and microwave absorbing properties of Ni–Zn spinel ferrites. *J Alloys Compd* 2009, **480**: 634–638.

[8] Grugeon S, Laruelle S, Dupont L, *et al*. An update on the reactivity of nanoparticles Co-based compounds towards Li. *Solid State Sci* 2003, **5**: 895–904.

[9] Larcher D, Bonnin D, Cortes R, *et al*. Combined XRD, EXAFS, and Mössbauer studies of the reduction by lithium of α-Fe_2O_3 with various particle sizes. *J Electrochem Soc* 2003, **150**: A1643–A1650.

[10] Alcántara R, Jaraba M, Lavela P, *et al*. $NiCo_2O_4$ spinel: First report on a transition metal oxide for the negative electrode of sodium-ion batteries. *Chem Mater* 2002, **14**: 2847–2848.

[11] Sharma Y, Sharma N, Subba Rao GV, *et al*. Nanophase $ZnCo_2O_4$ as a high performance anode material for Li-ion batteries. *Adv Funct Mater* 2007, **17**: 2855–2861.

[12] Zhou L, Zhao D, Lou XW. Double-shelled $CoMn_2O_4$ hollow microcubes as high-capacity anodes for lithium-ion batteries. *Adv Mater* 2012, **24**: 745–748.

[13] Borges FMM, Melo DMA, Câmara MSA, *et al*. Magnetic behavior of nanocrystalline $MnCo_2O_4$ spinels. *J Magn Magn Mater* 2006, **302**: 273–277.

[14] Lavela P, Tirado JL, Vidal-Abarca C. Sol–gel preparation of cobalt manganese mixed oxides for their use as electrode materials in lithium cells. *Electrochim Acta* 2007, **52**: 7986–7995.

[15] Rios E, Poillerat G, Koenig JF, *et al*. Preparation and characterization of thin Co_3O_4 and $MnCo_2O_4$ films prepared on glass/SnO_2:F by spray pyrolysis at 150 ℃ for the oxygen electrode. *Thin Solid Films* 1995, **264**: 18–24.

[16] Choi J-J, Ryu J, Hahn B-D, *et al*. Dense spinel $MnCo_2O_4$ film coating by aerosol deposition on ferritic steel alloy for protection of chromic evaporation and low-conductivity scale formation. *J Mater Sci* 2009, **44**: 843–848.

[17] Duan L, Jia S, Cheng R, *et al*. Synthesis and characterization of Co sub-micro chains by solvothermal route: Process design, magnetism and excellent thermal stability. *Chem Eng J* 2011, **173**: 233–240.

[18] Wang YQ, Cheng RM, Wen Z, *et al*. Synthesis and characterization of single-crystalline $MnFe_2O_4$ ferrite nanocrystals and their possible application in water treatment. *Eur J Inorg Chem* 2011, **2011**: 2942–2947.

[19] Zhou X-M, Wei X-W. Single crystalline $FeNi_3$ dendrites: Large scale synthesis, formation mechanism, and magnetic properties. *Cryst Growth Des* 2009, **9**: 7–12.

[20] Peng ZA, Peng X. Mechanisms of the shape evolution of CdSe nanocrystals. *J Am Chem Soc* 2001, **123**: 1389–1395.

[21] Peng ZA, Peng X. Nearly monodisperse and shape-controlled CdSe nanocrystals via alternative routes: Nucleation and growth. *J Am Chem Soc* 2002, **124**: 3343–3247.

[22] Zhao L, Zhang H, Tang J, *et al*. Fabrication and characterization of uniform Fe_3O_4 octahedral micro-crystals. *Mater Lett* 2009, **63**: 307–309.

[23] Hou X, Feng J, Xu X, *et al*. Synthesis and characterizations of spinel $MnFe_2O_4$ nanorod by seed–hydrothermal route. *J Alloys Compd* 2010, **491**: 258–263.

[24] Duan L, Jia S, Cheng R, *et al*. Synthesis and characterization of Co sub-micro chains by solvothermal route: Process design, magnetism and excellent thermal stability. *Chem Eng J* 2011, **173**: 233–240.

[25] Ai L-H, Jiang J. Rapid synthesis of nanocrystalline Co_3O_4 by a microwave-assisted combustion method. *Powder Technol* 2009, **195**: 11–14.

[26] Li ZH, Zhao TP, Zhan XY, *et al*. High capacity three-dimensional ordered macroporous $CoFe_2O_4$ as anode material for lithium ion batteries. *Electrochim Acta* 2010, **55**: 4594–4598.

[27] Kang Y-M, Song M-S, Kim J-H, *et al*. A study on the charge–discharge mechanism of Co_3O_4 as an anode for the Li ion secondary battery. *Electrochim Acta* 2005, **50**: 3667–3673.

[28] Lavela P, Ortiz GF, Tirado JL. High-performance transition metal mixed oxides in conversion electrodes: A combined spectroscopic and electrochemical study. *J Phys Chem C* 2007, **111**: 14238–14246.